Biomaterials 82 (2016) 113–123

Contents lists available at ScienceDirect

Biomaterials

journal homepage: www.elsevier.com/locate/biomaterials

Phototriggered fibril-like environments arbitrate cell escapes and migration from endothelial monolayers

Marcelo J. Salierno [a, b, *], Luis García-Fernandez [a], Noelia Carabelos [a, b], Karin Kiefer [d], Andrés J. García [c], Aránzazu del Campo [a, d, e, **]

[a] Max-Planck-Institut für Polymerforschung, Ackermannweg 10, 55128, Mainz, Germany
[b] Department of Biological Chemistry, School of Sciences, University of Buenos Aires, IQUIBICEN-CONICET, CABA, Argentina
[c] Woodruff School of Mechanical Engineering and Petit Institute for Bioengineering and Bioscience, Georgia Institute of Technology, Atlanta, GA, 30332, USA
[d] INM – Leibniz Institute for New Materials, Campus D2 2, 66123, Saarbrücken, Germany
[e] Saarland University, Campus Saarbrücken D2 2, 66123, Saarbrücken, Germany

ARTICLE INFO

Article history:
Received 8 December 2015
Accepted 12 December 2015
Available online 17 December 2015

Keywords:
Cell migration
Endothelial transition
Cyclic RGD
Photoactive materials

ABSTRACT

Cell detachment and migration from the endothelium occurs during vasculogenesis and also in pathological states. Here, we use a novel approach to trigger single cell release from an endothelial monolayer by in-situ opening of adhesive, fibril-like environment using light-responsive ligands and scanning lasers. Cell escapes from the monolayer were observed on the fibril-like adhesive tracks with 3–15 μm width. The frequency of endothelial cell escapes increased monotonically with the fibril width and with the density of the light-activated adhesive ligand. Interestingly, treatment with VEGF induced cohesiveness within the cell layer, preventing cell leaks. When migrating through the tracks, cells presented body lateral reduction and nuclear deformation imposed by the line width and dependent on myosin contractility. Cell migration mode changed from mesenchymal to amoeboid-like when the adhesive tracks narrowed (≤5 μm). Moreover, cell nucleus was shrunk showing packed DNA on lines narrower than the nuclear dimensions in a mechanisms intimately associated with the stress fibers. This platform allows the detailed study of escapes and migratory transitions of cohesive cells, which are relevant processes in development and during diseases such as organ fibrosis and carcinomas.

1. Introduction

Endothelial cells are recognized as a source of cancer associated fibroblasts (CAF), accounting for the up to 40% of CAF found in tumors [55], in cardiac and pulmonary fibrosis [39] and tissue malformations [31]. Although this phenomenon is well documented, the critical factors that motivate and guide single cells to escape the endothelial monolayer, migrate into the stroma and transform into a different phenotype remain unclear.

Migration studies over the last decade have demonstrated that the molecular composition of the ECM and its architectural parameters like rigidity, density or topology of its constituting fibers are key variables of the migration environment [4,13]. Cells change their migration behavior to adapt to the different microenvironments using their contractile cytoskeleton in coordination with extracellular guidance cues. For simplicity, cell migration modes can be described as individual (i.e., amoeboid or mesenchymal) or collective (i.e., movement of coupled cells) migration [14]. In reality, cells adopt intermediate and interconvertible modes between states depending on the surrounding matrix.

Accruing evidence demonstrate that the topology of ECM fibers (diameter, aligned or random orientation) is a key parameter that forces cells to modify their migration properties [2–4,8,11,14,22,25,53,54]. Also, changes in ECM fibers occur under pathological conditions [12,14,29] and can trigger migratory transitions of embedded cells and modify invasive efficiency and metastasis occurrence [30]. Recent studies have shown that non-migrating cells undergoing a mesenchymal transition can

Abbreviations: CAF, cancer associated fibroblasts; ECM, extracellular matrix; FAs, focal adhesions; HUVEC, human umbilical vein endothelial cells; IS, instantaneous speed; nLA, nuclear long axes; nSA, nuclear short axes.

* Corresponding author. Max-Planck-Institut für Polymerforschung, Ackermannweg 10, 55128, Mainz, Germany
** Corresponding author. INM – Leibniz Institute for New Materials, Campus D2 2, 66123, Saarbrücken, Germany
E-mail addresses: salierno@mpip-mainz.mpg.de (M.J. Salierno), delcampo@leibniz-inm.de (A. Campo).

http://dx.doi.org/10.1016/j.biomaterials.2015.12.001
0142-9612/

experience a transition to amoeboid motility under confinement in a low adhesive environment [18,28]. Intermediate states between mesenchymal and amoeboid migration modes were observed upon changes in the concentration of adhesive ligands [28] or changes in the density, porosity and stiffness of the ECM during cancer progression [53].

Migration along aligned collagen fibers is crucial in tumor cell spreading [16,36], and aligned matrices were useful strategies for directing stem cell migration after transplantation into the rat auditory nerve and after spinal cord injuries [8,33,47]. Fiber-guided migration has been studied by seeding cells on planar substrates micropatterned with adhesive lines [8,9,32,38]. This simplified 1D microenvironment has been demonstrated to be an appropriate model to study cell migration along ECM fibers in 3D contexts, as it happens *in vivo* [36]. Escape and migration of cells out of a cohesive cell layer can also be studied in vitro by first spatially confining a group of cells and providing them free adhesive areas later. This is typically achieved using physical barriers, i.e. a PDMS block that confines cells in a reservoir and, when removed, allows cell expansion into new areas [10]. Physical barriers have also been combined with microcontact printed adhesive lines to expose cell in a monolayer to fiber-like adhesive tracks [50].

Whereas these methods have achieved remarkable results in explaining collective and single cell migration response in the new adhesive spaces, they have limited applicability to study the initial stages of the migration process, i.e. the cell–cell detachment event from the preformed layer and the cell changes when entering the confined 1D environment, and their dependence on geometrical and biochemical effectors. In this context, here we present a method that precisely regulates adhesive space in time and with defined geometries and ligand density, and offers constant monitoring of the cell escape process. It represents a new biomaterial platform that allows to phototrigger cell migration *in situ* [42]. It makes use of surface layers containing a photo-activatable adhesive peptide (cRGD) that binds integrin receptors at the cell membrane only after light exposure [52]. Localized exposure allows generation of cell-adhesive domains to which cells can attach and spread forming confined monolayers within a non-adhesive surrounding. In a second exposure step, adhesive microlines of desired geometry can be opened in-situ using a scanning laser. Here, we apply this methodology to study endothelial escapes and migration from a confined monolayer into fiber-like environments. We reveal the relevant role of the fiber diameter together with the adhesive ligand density in the activation of endothelial cell escapes as well as in their subsequent migration mode. Our studies provide insights on the role of ECM spatial organization in promoting cellular escapes and transitions modulated by the width of the fibrillary tracks, the density of the ligand and the presence of the external factors.

2. Results

2.1. Endothelial escapes can be photo-triggered in situ in the range of 3–15 μm linewidth

Patterned monolayers of endothelial cells were generated by culturing HUVECs on mask-irradiated substrates modified with photo-activatable RGD (Fig. 1a). The activated RGD pattern guided the formation of confined cell monolayers in the form of stripes. Cell monolayers remained confined to photo-activated patterns for more than 3 days under time lapse (movie 1), demonstrating that these substrates are suitable for long term microscopy studies. Migration lines were opened from the confined monolayers by scanning lines orthogonal to the pattern edge across the cell-free space using the 405 nm (5 mW) laser beam from the microscope (Fig. 1b). Cellular escapes from the monolayer and subsequent migration into adhesive lines of different widths was followed by time-lapse microscopy (Fig. 1c).

Supplementary data related to this article can be found online at http://dx.doi.org/10.1016/j.biomaterials.2015.12.001.

Migration on lines wider than 15 μm mainly involved collective migration: the leader cell remained attached to the neighbors and protrusion of the monolayer was observed on the lines (Fig. 1c top panel), in agreement with previously reported data [42,50] and following a similar behavior recently described as epithelial bridges [49]. On lines narrower than 15 μm, cells spread through the entire width of the line, polarized, detached from the monolayer, and migrated as single cells (movie 2). No escape events were observed on lines narrower than 3 μm. These results demonstrate that the width of the adhesive path significantly influences endothelial escape, which occurs in our platform within the narrow range from 3 to 15 μm.

Supplementary data related to this article can be found online at http://dx.doi.org/10.1016/j.biomaterials.2015.12.001.

2.2. Escaping cells form focal adhesion within the adhesive paths with fast front-rear aggregation

Single migrating cells strictly adapt their contour to the irradiated areas. Visualization of the focal adhesions (FAs) (cells transfected with GFP-vinculin plasmid) showed that mature FAs were only formed within the adhesive pathway (SI1e). Occasional spreading of the cell rim outside of the scanned areas was observed when transient blebs formed but disappeared soon afterwards because of lacking stable substrate interactions. In order to analyze the evolution of the adhesive contacts during cellular escapes, mature FAs were followed during single cell break into the lines by using a GFP-Vinculin construct. Fig. 1d and e shows confocal images of the FAs of a migrating cell from the endothelial monolayer to an open space or to a confined situation respectively. Distribution of the mature FAs was further quantified and analyzed by applying an aggregation index. Fig. 1f and g, show a heat map of the areas with highest vinculin density (red spots) corresponding to the location of the most mature FAs considered for analysis. A random distribution of FAs was found when cell migrated in an open space, with no particular FAs aggregation. In contrast, cells migrating in confined tracks showed aggregated FAs ($I \leq 0.05$), mostly accumulated at the front and at the rear.

2.3. Endothelial escape events are modulated by line width, ligand density and external factors

The number of escape events in which endothelial cells detached the confluent monolayer and entered to the migration lines was quantified (Fig. 2a and b). Endothelial escapes were scarce on 3 and 5 μm-width. In these cases, cells constantly attempted to enter the path, but most of them were unable to detach from the monolayer and initiate migration. The number of cell escapes into the adhesive lines increased monotonically with the line width (Fig. 2b), with significant difference between cells escaping on lines of 10 and 15 μm width and those on lines with 3 and 5 μm width. The density of adhesive ligand also affected the number of endothelial escapes (Fig. 2c). By increasing the exposure dose on the scanned spaces, a notable 2.5 fold increase in the number of escapes was observed was observed on lines of 10 μm. Cells were less sensitive to ligand density changes on lines of 5 μm-width, with a total increment of 0.9-fold within the tested density range. Notice that the line width became a more relevant factor to trigger cell escapes at increasing adhesive ligand density. The reduced cells sensitivity to ligand density on narrow lines is in agreement with

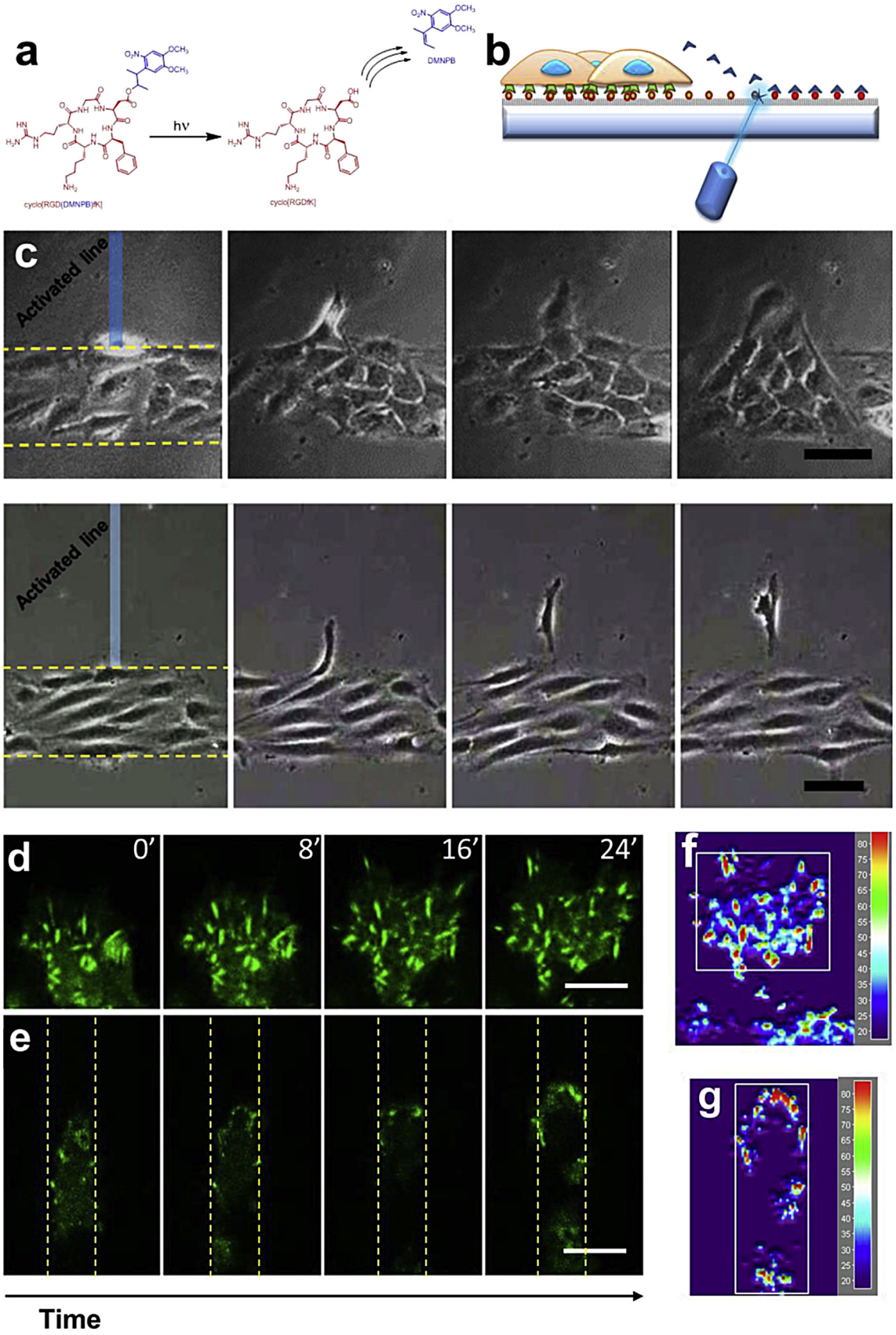

Fig. 1. Directing cell escapes from an endothelial monolayer. a- Photo-activatable cyclo[RGD(DMNPB)fK] before and after irradiation. b- Illustrative scheme of the photoactivation of a migratory pathway by laser scanning at the cell monolayer border. c- Image sequence showing the influence of the line width in triggering collective (top, 20 μm-width) or single (bottom, 10 μm-width) endothelial cell migration from a preformed monolayer. Pictures are shown every 1 h. Scale bar 50 μm. Image sequence of FA (in green) taken every 8 min after RGD activation. d- FA of a cell migrating across a wider line providing no confinement. Stable Mature FAs appears randomly distributed, new FAs progress by widening

the findings that in 1D migration cells are not sensitive to ligand density [9]. In our case, lines of 3–5 μm-width are closer to resemble a 1D situation compared to cells on lines of 10–15 μm-width.

Additionally, to compare directly in which extent the line width can exert endothelial cell polarization and migration *per se* we seeded the cells directly on irradiated lines. On lines of 1.5 and 3 μm-widths, cells were unable to generate cell adhesion and spreading. Lines above 5 μm-widths succeeded in inducing cell attaching, spreading and polarization with remarkably high efficiency on lines of 10 and 15 μm (SI2 a and b). This indicates that the competence of cells to adhere and spread on lines are compromised as the lines are getting narrow suggesting that the differences in generate cell–cell breaking events by different linewidth can be closely associated with this phenomenon.

We also evaluated whether the cutoff of endothelial escapes at 3 μm-width is characteristic of a cell type, or if it can be decreased in a less cohesive cell line. For this purpose, we used HT1080 fibroblasts. These cells were able to enter to lines as narrow as 1.5 μm (SI2c, movie 3). Notably, HT1080 fibroblasts exhibited a lower sensitivity to line width and a significantly higher number of cell escapes (20 times higher on 5 and 3 μm-widths) compared to endothelial monolayers (SI2d).

Supplementary data related to this article can be found online at http://dx.doi.org/10.1016/j.biomaterials.2015.12.001.

We evaluated cell escapes under the influence of VEGF as external factor that promotes migration and proliferation in endothelial cells. Interestingly, collective cell migration was observed on lines of 10 μm-width (SI2e). This is in agreement with the multiple roles that VEGF has in cellular behavior depending of the context of the microenvironment [17]. Although more research should be done in this direction, these data demonstrate the relevance of our platform to explore endothelial escapes or sprouting on defined adhesive contexts combined with soluble factors.

2.4. Single cell migration mode is altered with the linewidth

Cells migrating on 10 and 15 μm wide lines had a polarized cell body with a well defined lamellipodium at the front. In these cases, cells moved slowly and smoothly along the line, without changing migration directions (Fig. 3a, movie 4). This migration mode resembled mesenchymal migration [14]. Remarkably, a different migration behavior was observed on narrow lines below 5 μm-width (Fig. 3b, movie 5). In this range, cells moved faster and changed migration direction frequently. During migration, cells showed small or no clear lamellipodium at the front. The cell body underwent dramatic changes in length while moving: it became occasionally highly elongated or short and rounded, displaying blebs at the membrane surface. These morphological features resemble a mesenchymal-amoeboid migration mode [13,34].

Supplementary data related to this article can be found online at http://dx.doi.org/10.1016/j.biomaterials.2015.12.001.

Cell migration features like instantaneous speed (**IS**), persistence or the effective distance away from the monolayer changed dramatically on lines of 5 and 10 μm widths. Representative image series of the cell crawling show high directional persistence of cells on 10 μm lines (Fig. 3a), and a dramatic reduction in persistence on narrower lines (Fig. 3b). We also estimate the cell directional persistence along the lines by counting the number of times that cells changed their direction along 12 h. On 5 μm lines, cells reversed the direction of migration almost 10-times more than on 10 μm lines (6.2 ± 1.4 vs. 0.7 ± 0.5 times/h respectively, $p < 0.002$). The arbitrary direction of motility for cells on 5 μm lines vs. the consistent forward motion of cells on 10 μm lines was also reflected by measuring 5 min interval displacements (Fig. 3c). In this graphic, negative values represent backward movements, which appear with nearly the same number and magnitude than the forward movements in the 5 μm lines. In addition, the instantaneous speed was significantly higher in cells migrating on 5 μm lines (Fig. 3d). Notably, although the 5 min displacements are higher in narrow lines, the effective distance that cells can migrate away from the monolayer is significantly smaller compared to the smooth, forward crawling cells on broader lines. Fig. 3e compares the migration trajectory of a cell on 5 and 10 μm lines over 12 h. As a consequence of their fast and non-directional movement, cells on 5 μm lines do not travel farther away from the monolayer (left) in spite of covering larger distances (right). In summary, cells migrating on 10 μm lines have lower **IS** but higher migration persistence, which results in the cell migrating farther away from the monolayer. Similar differences in the migration behavior were also observed for cells on 3 and 15 μm lines.

Interestingly, similar differences in migration speed were also reported for fibroblast on lines with widths between 1 and 40 μm. The migration speed of fibroblasts on lines with width below 2.5 μm was low, it increased significantly for lines between 2.5 and 5 μm, and it decreased again on wider lines [9]. However, no indications on the migration mode were made in this report. Our results indicate a correlation between the observed speed differences and a line-width dependent transition of the migration mode. Moreover, these results demonstrate that single cell migration on lines narrower than 5 μm occurs with high speed but low persistence. However, on the range of 10–15 μm line width, where cells showed clear characteristics of mesenchymal migration, although speed decrease persistence increase making migration more efficient in terms of migration distance from the monolayer.

We also studied the nature and distribution of FAs on the adhesive tracks of different widths. The number of FAs significantly decrease on confinement in general and even less on tracks of 5 μm-width comparing with 10 μm-width (SI3 a and b), in agreement with previous work [3]. These differences are reflected in the observed cell migration modes. The reduced amount of focal points on narrower tracks mediates weak cell attachment and the transition from mesenchymal to amoeboid migration. We believe that cell escape modulation by geometry and the fact that the line width forced cells to adopt different migration modes emphasize the idea that ECM changes are related to disease progression. In this context, the surrounded adhesive fibers during tissue repair, carcinogenesis or fibrosis may turns as potential responsible of cellular leakage, transition and dispersion.

2.5. Cell body and nuclear shape shrank laterally reaching DNA compaction on lines ≤5 μm width

Cells adjusted their shape and dimensions in response to the width of the adhesive lines. Fig. 4a presents images of the actin cytoskeleton of cells on 5 and 10 μm lines and a cell on an unpatterned surface. Cells spread area was significantly reduced on cells migrating on the lines comparing with cells on an unpatterned

the leading front without a specific pattern. Typically collective migration is followed. e- Cell migrating over a 10 μm line with mature FAs (bright green) distributed mostly at the cell rim. The more stable FAs remains at the edge in this case single cell migration follows. Scale bar 15 μm. Heat map showing FAs distribution in unconfined (f) and confined cell (g). The white box encloses the area where the mature FAs (in red) are scattered. (For interpretation of the references to color in this figure legend, the reader is referred to the web version of this article.)

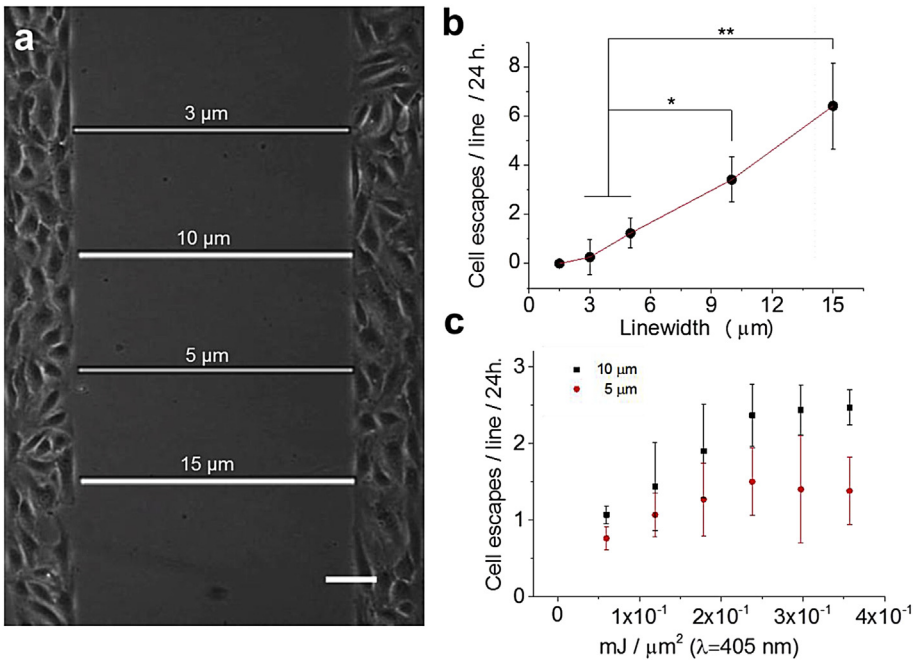

Fig. 2. Migration events are line width dependant. a- Design of the second step irradiation of lines to direct SCM from a HUVEC monolayers on strips HUVECs monolayers spaced by 400 μm. Lines of different thickness were irradiated perpendicular to the strips. Scale bar 100 μm. Quantitative analysis of SCM along line patterns with increasing width: b- Cell migration events depending of the line width during 24 h. Data are means ± SD of 3 independent experiments with 6 replicates. c- Cellular escapes on line widths of 10 and 5 μm were evaluated under increasing activation of cRGD controlled by several scans of same laser energy dosage of 0.06 mJ/μm^2. Data are means ± SD of 2 independent experiments with 4 replicates each. Cell migration speed as a function of line width. UP: unpatterned. **: $P < 0.01$, *: $P < 0.05$.

space. Cell spread area decreased to 30% of the average size in 10 μm lines and to 12% in 5 μm lines when compared to unpatterned spreading (Fig. 4b).

This body reduction also impacts on the cell nucleus which underwent significant dimensional changes during migration in confinement. Fig. 4c shows images of the nucleus of cells migrating on 10 and 5 μm lines and that of a cell within the monolayer. When the cells are part of the endothelial monolayer, nuclear shape can be described as an ellipse (see scheme in Fig. 4d) with a short (**nSA**) and a long axes (**nLA**). The nucleus of cells migrating on the lines oriented the **nLA** along with the migration direction and had a more pronounced ellipticity than the nucleus of cells in the unpatterned area. The length of the nuclear axes in HUVECs in an unconfined space displayed a normal distribution (Fig. 4d) with a mean length of $\mathbf{nSA_{UP}} = 14.3 \pm 2.1$ μm, and $\mathbf{nLA_{UP}} = 22.0 \pm 1.9$ μm. The length of the **nLA** of cells on unpatterned and on 10 μm lines showed no significant differences ($\mathbf{nLA_{10\mu m}} = 20.6 \pm 2.3$ μm). However, $\mathbf{nSA_{10\mu m}} = 8.30 \pm 1.7$ μm was significantly shorter than $\mathbf{nSA_{UP}}$ (Fig. 4e). A radical reduction in the nuclear dimensions was observed in cells migrating on 5 μm lines, with $\mathbf{nSA_{5\mu m}} = 5.16 \pm 1.6$ μm and $\mathbf{nLA_{5\mu m}} = 15.8 \pm 2.2$ μm. In general, we observed **nSA** of endothelial cells migrating under line confinement shrank to the width of the line. However, this did not occurred in cells migrating on 3 μm lines, where $\mathbf{nSA_{3\mu m}} \sim 4$ μm. We believe that this limit in the nuclear contraction of endothelial cells affects adhesion (SI2c) and migration that started to transit to an amoeboid state on lines of 5 μm-width and unable below 3 μm-width. Interestingly, the $\mathbf{nSA_{3\mu m}}$ limit was similar to that reported for cancer cells in 3D collagen matrix [19,53]. Furthermore, DAPI staining displayed higher fluorescence intensity in the nucleus of cells migrating on 5 μm lines confirming chromatin condensation (Fig. 4f). Additionally, on line widths ≤5 μm cells displayed many blebs on the membrane (Fig. 5a arrows head and see SI4 and movie 6) as another sign of amoeboid migration mode or an intermediate mesenchymal-amoeboid state.

Supplementary data related to this article can be found online at http://dx.doi.org/10.1016/j.biomaterials.2015.12.001.

All this features suggests that the cell adaptation to the narrow tracks could have dramatic implications at gene transcriptional levels [41,45]. Although more research needs to be done, this morphological change can be decisive or necessary for particular cases of cellular transitions.

2.6. Nuclear contraction is linked with the distribution of lateral stress fibers and requires myosin contractility

The spatial distribution of stress fibers is influenced by the cell shape and spreading [51,56]. The actin cytoskeleton of an endothelial cell migrating on unpatterned spaces showed actin fibers distributed throughout the cell spread area (Fig. 5e). When the cells migrated on the tracks, a reduction in the density of the stress fibers of the actin cytoskeleton was observed. A confocal z-stack of actin in cells on 5 and 10 μm lines (Fig. 5a and b respectively) showed most of the actin fibers distributed laterally, with transverse short fibers at the frontal lamellipodia. For cells on 5 μm lines, a 3D reconstruction image (Fig. 5a and movie 6) showed no apparent transverse-arc-like stress fibers in migrating cells. Ventral, dorsal and perinuclear stress fibers are normally observed during migration over unpatterned substrates [23,46]. In our case, these types of fibers converged into lateral fibers crossing the entire length of the cell, in a similar but simpler arrangement than in cells on 10 μm lines. Cell nucleus appears laterally squeezed with a strong deformation at the level where the longitudinal stress fibers are placed (SI4).

Myosin II is required for efficient migration in 1D geometries, whereas actomyosin contractility was not required for unconstrained migration [7]. In fact, inhibition of actomyosin contractility by blebbistatin treatment enhanced migration in an unpatterned

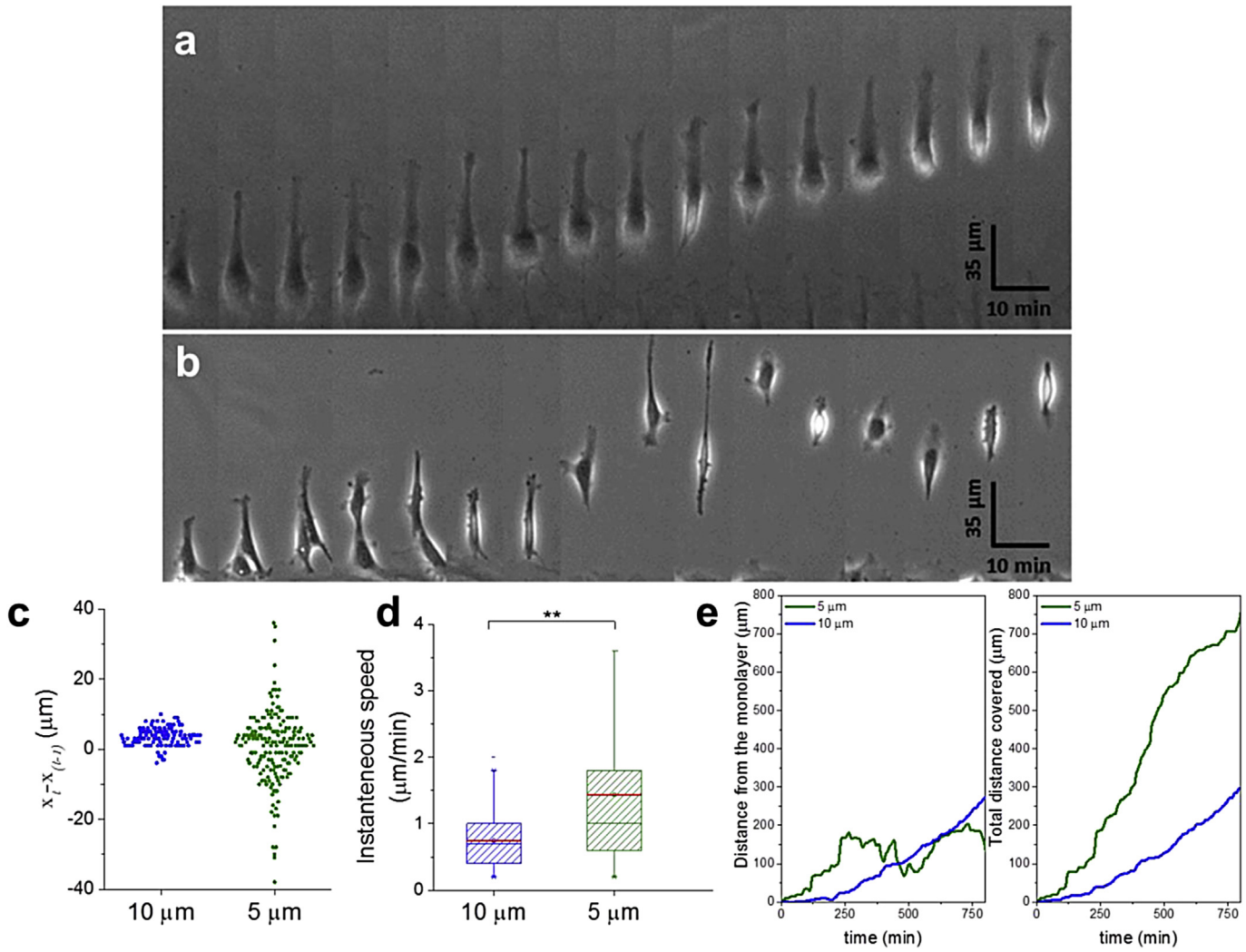

Fig. 3. Endothelial morphology along linear paths of different thickness. Representative short-timescale image sequences from time-lapse movies of HUVECs migrating along 10 μm (a), 5 μm (b) thick lines. The images depict variations in cell shape, crawling and migration persistence along the time. Cell migrating on 5 μm shows low persistence and large variations in body size and shape while cells crawling on 10 μm show appreciable high persistency and almost invariable body length. c- Absolute distance covered by cells at intervals of 5 min over 10 and 5 μm line widths where cell direction changes can be seen on the negative measurements. d- Box plot shows instantaneous speed (IS) variability that significantly increase in 5 μm comparing with 10 μm line widths (Kruskal–Wallis **: $P < 0.01$). Data are from 2 independent experiments with 3 replicates each. e- Representative path of the distance from the monolayer (left) and accumulated displacement (right) vs time of over a representative cell migrating on 5 and 10 μm line widths during 12 h.

space [9]. We evaluated the role of actomyosin contractility in experiments using blebbistatin (10 μM). Although migration was impaired, treatment with blebbistatin resulted in the formation of blebs in cells on 10 μm lines, but the shape and the cell length remained unmodified (Fig. 5e, second column). On 5 μm lines, blebbistatin treatment promotes detachment when cells are not stretched and dramatically changed the shape on elongated cells, indicating that the contributions of actomyosin contractility in regulating cell shape and stabilize attachment became more relevant with increasing confinement. Furthermore, the nuclear dimensions of cells on 5 μm lines were strongly affected upon blebbistatin treatment: **nSA** increased in ~60% ($\mathbf{nSA_{5\mu m\ bleb}} = 7.61 \pm 1.4$ μm, $p < 0.01$) and **nLA** shrank in ~20% ($\mathbf{nLA_{5\mu m\ bleb}} = 12.48 \pm 2.6$ μm, $p < 0.001$). Cells migrating on 10 μm lines did not show significant changes in **nSA**, and a less pronounced but significant change in **nLA** ($p < 0.05$) (Fig. 5f and g). A similar response was found in unconfined cells.

Nuclear deformation can be critical in regulating not only cell migration but also cell fate [15,24]. We analyzed the relationship between the size of the long and short nuclear axes (**nLA, nSA**) and the cell body length. The correlation between the body length and the nuclear dimensions was stronger in cells on narrower lines (Table 1 and SI5), under blebbistatin treatment, this correlation was abolished for cells on 5 μm lines and partially impaired in cells on 10 μm lines (SI5). These results confirm a fundamental role of actomyosin filaments in reshaping the nucleus on cells on narrower lines and a partial role for nuclear stretching on thicker lines. Also, these results suggest that nuclear compression is forced during cell stretching by the contraction of the lateral actomyosin fibers. Summarizing, we found the actin cytoskeleton critically involved in nuclear deformation on single endothelial cells migrating on the narrow lines. Actomyosin contractility seems to be the mechanisms that cause lateral deformation of the nucleus under uniaxial confinement, and it has a crucial role in retaining cell during migration under narrower lines.

3. Discussion

Using a novel photoactivatable biomaterial, we have studied the response of endothelial monolayers to the emergence of fiber-like

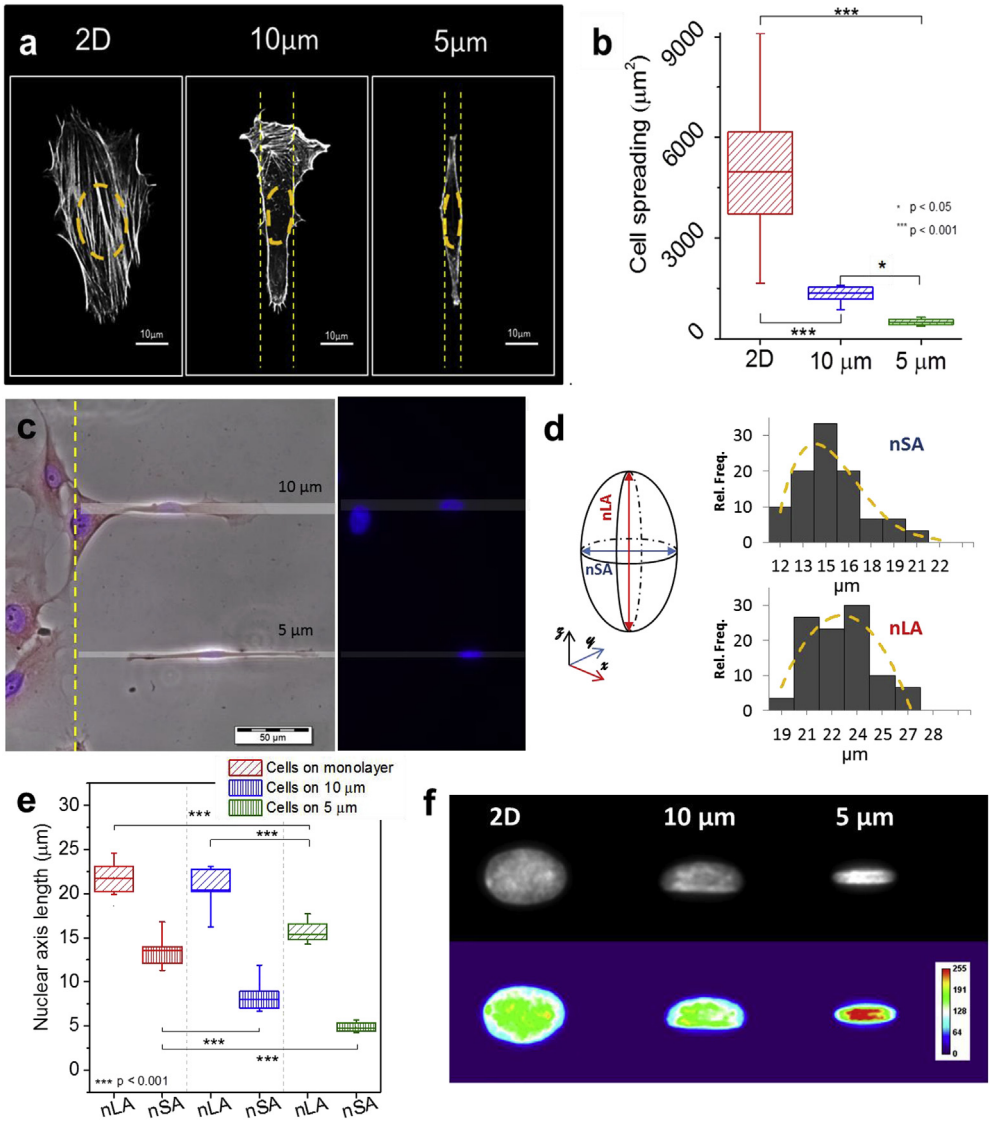

Fig. 4. Body and nuclear spreading are reduced following line confinement. a- Fluorescent images of the cytoskeletal actin filaments stained on cells polarized in unpatterned areas, or 10 and 5 μm line widths, nucleus are delimited in red dash line, scale bar 10 μm. b- Average cell area on unpatterned spaces and 10 μm and 5 μm lines. c- Lateral compression of the nuclei (DAPI staining in blue) fit the path over 10 μm and 5 μm line width during cell crawling. d- Frequency distribution of short (nSA) and long (nLA) nuclear axis (scheme) in HUVECs cells on a monolayer. e- nSA and nLA box plot on cells under migration on 10 μm or 5 μm line widths. f- Heat map of chromatin contents measured by DAPI staining on unpatterned; 10 and 5 μm show chromatin condensation on nuclei under 5 μm paths. ***: $P < 0.001$. (For interpretation of the references to color in this figure legend, the reader is referred to the web version of this article.)

migration spaces at the monolayer boundary. This biomaterials platform allows great flexibility in the design parameters of the migration space, including dimensions and geometry, density and time-resolved availability of adhesive ligands. Notably, light mediated activation of migratory spaces increases accuracy and improves *in situ* manipulation during time lapse microscopy, not possible with other techniques such as physical barriers [10,50]. Our platform presents, for the first time *in situ* patterning and modulation of adhesive ligand density on pre-established cell cultures.

Surprisingly, endothelial cells, which typically undergo collective migration, escape as single cells on lines of few microns of adhesive spaces. Moreover, we found that the choice of an endothelial cell to leave the monolayer and initiate single cell migration on micrometric tracks are restricted to a range of few microns (15–3 μm line width) with high variability and responsive to the ligand density. This is a relevant feature to be considered when conducting studies of cell migration or cell adhesive response, since this factor may not easy to define and control in other experimental approaches.

In this scenario, cell escapes becomes more frequent as lines became thicker (Fig. 2b) and cell escape rises as the activated ligand density is increased (Fig. 2c). This can be associated to the fact that the cell can build and generate more stable forward forces at the lamellipodium increasing the chance of cells to overcome the cell–cell interaction. It has been demonstrated that directional persistence in cell migration correlates with the front lamellipodial stability [20] and that stability strongly depends on stable integrin binding [26]. In our case, both processes are reduced as patterns become narrower.

Also, when migrating on adhesive lines, endothelial cells show width-dependent migration behavior changing significantly on lines with widths between 5 and 10 μm. Cell speed increased (high **IS**) but persistence declined when cells become narrower. On lines

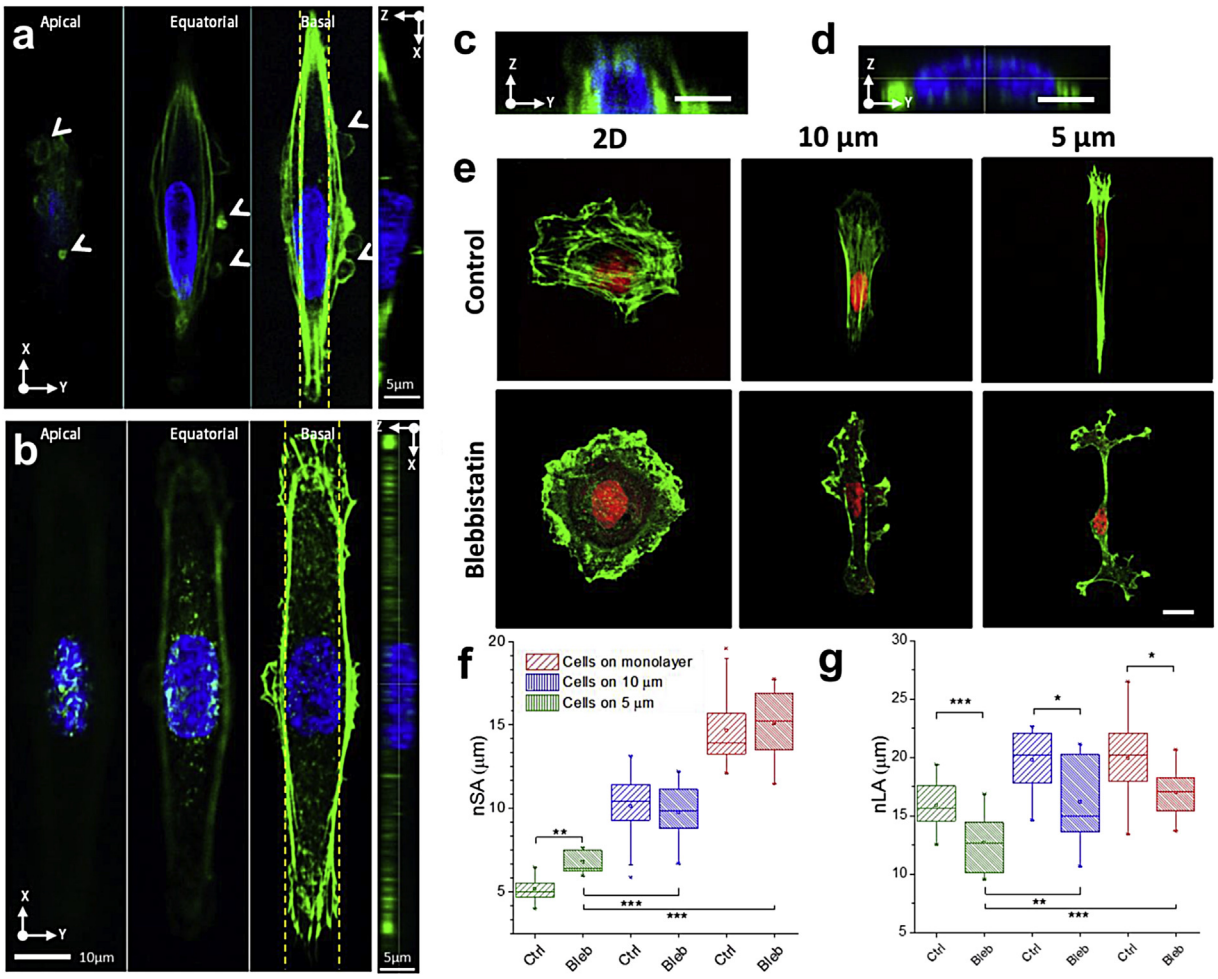

Fig. 5. Lateral stress fibers and myosin contractility are closely linked with the nuclear deformation. Representative confocal microscopy Z stack of actin scaffold (green) and nuclear shape (blue). Sections along the apical, equatorial, basal surfaces and equatorial cross section along XY, XZ and ZY plane of cells on 5 (a and c) and 10 μm line width (b and d). For HUVEC 3D reconstruction on 5 μm line width patterns. Head arrows indicate clear blebs at the membrane surface over the cell membrane on 5 μm line width. RGD patterns are indicated with yellow dashed lines. Equatorial cross sections show lateral compression in close connection by the surrounded lateral stress fibers (movie 6). e- HUVEC morphology on unpatterned and on line patterns with or without blebbistatin 10 μM. Actin appears in green and nucleus in red. Scale bar 10 μM. Statistical analysis of nuclear axis changes with or without blebbistatin 10 μM (f and g nSA and nLA box plot respectively) on cells under migration on unpatterned surface (red), 10 μm (blue) and 5 μm (green) line widths (***: $P < 0.001$, **: $P < 0.01$, *: $P < 0.05$). (For interpretation of the references to color in this figure legend, the reader is referred to the web version of this article.)

Table 1
Cell body length correlation with nuclear long and short axis. Statistical correlation between body length and nuclear long (**nLA**) and short (**nSA**) axis was evaluated on 5 and 10 μm line widths as well as in unpatterned cells. The table shows a raise in the correlation with increasing restriction of the patterns only for **nLA**. Under blebbistatin treatment **nLA** correlation on 5 μm line width is reduced dramatically.

Correlation of nuclear dimensions vs. body length			
	2D	10 μm	5 μm
nLA	0.14	0.52	0.74
nSA	0.24	0.56	0.59
Blebb nLA		0.48	0.25

<5 μm width, cells showed blebs at the membrane (Fig. 5a), and underwent cycles of elongated and rounded cell body shape (Fig. 3b). This behavior is characteristic of a mesenchymal-amoeboid transition, and can be attributed to a decrease in the stability of the lamellipodium as a consequence of the lower lateral spreading in narrow lines [26]. The change between mesenchymal and amoeboid migration modes and the existence of intermediate states depending on Rac1/RhoA activity has been recently demonstrated [21]. Other reported studies have that cells switch to amoeboid migration mode under confinement in low adhesive pathways [14,18,22,25]. In our experiments, endothelial cells on lines of ≤5 μm-width shown an intermediate state of mesenchymal-amoeboid migration.

Remarkably, the transition of an endothelial cell from being part of the monolayer to undergo a single cell migration mode involves a significant shrinkage of the cell body and a profound cytoskeletal rearrangement resulting in nuclear reshaping and shrinkage to adapt to the geometrical restriction imposed by the adhesive path (Figs. 4 and 5). We summarize this in Fig. 6 and Table 2, the photo-activated cyclicRGD adhesive line represents a uniaxial assembly of adhesive ligands that induces polarization, nuclear contraction and squeezing of the cell to adapt to the adhesive pattern, independently of 3D-spatial limitations and similar to previous reports on fibronectin fibers [57]. Our studies suggest that the spatial arrangement of the adhesive ligands to which the cell attaches and pulls on for forward movement, i.e. the ECM fiber geometry in a 3D *in vivo* context, may play a critical role in determining cell escapes and the ability of the cell to shrink the nucleus and migrate in confined spaces. Although is not clear whether nuclear

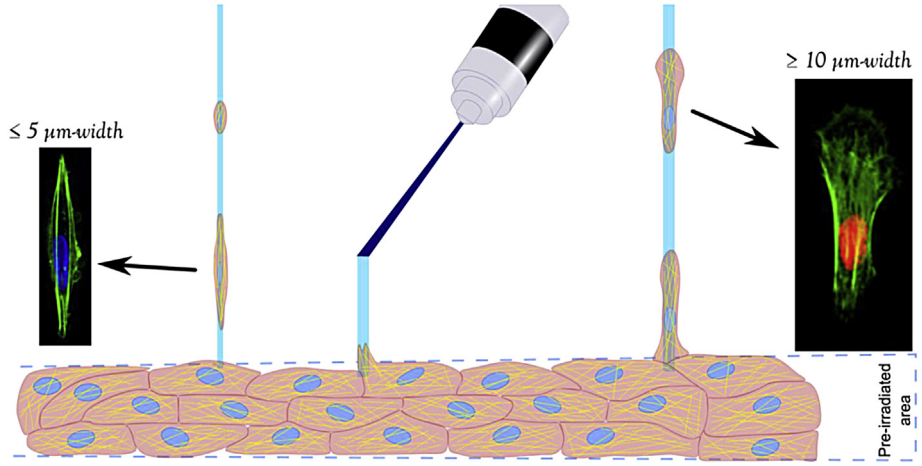

Fig. 6. Representative diagram of the experimental conditions after different uniaxial stimulation that trigger cell escapes.

Table 2
Comparison of the cell migration properties after being directed from the monolayer with different areas of ligand availability.

Cell migration on lines	Width (μm)	Lateral cell body	Nuclear dimensions		DNA compaction	Amoeboid features	Miosin contraction dependence
			nLA	nSA			
Unpatterned	–	Spread	22.0 ± 1.9	14.3 ± 2.1	No	No	No
Wide	10–15	=Line width	20.6 ± 2.3	8.30 ± 1.7	No	No	Moderate
Narrow	3–5	>Line width	15.8 ± 2.2	5.26 ± 0.6	Yes	Blebs	High

deformation is part of the process or a consequence of the cytoskeletal reassembly during line confined migration, they are closely linked and both seems to be necessary for migration on paths narrower than the nuclear shape. We hypothesize narrow patterns can trigger single cell migration by forcing a rearrangement of the cytoskeleton which is reflected in FAs aggregation (see also section 2) at the extremes and edges as soon as the cell enter to the track. Consequently, spaces larger enough to avoid cell body lateral confinement (in our case above 15 μm-width) should prevent cell escapes and induce a typical collective migration instead.

Moreover, the drastic reduction in the cell size induced by the confinement of adhesion spaces can facilitate migration of cells along adhesive fibers within 3D environments with pores smaller than the average cell size. In a different context, our results suggest that the probability of single cells to leave a cell layer and initiate migration through a fibrillar environment strongly increases with the diameter of the fibers. Interestingly, rearrangement and dimensional changes of ECM fibers in tumor microenvironments has been demonstrated to correlate with invasiveness [27,37,40]. Our data support these findings and provides length scales for a better understanding of the correlation between ECM topology and tissue disease progression.

These results suggest that the arrangement of ECM fibers can be a powerful regulator of migration *in vivo*, in agreement with recent evidence that ECM plasticity and dimensionality dictate the migration modes [14]. In particular, our photo-triggerable migration lines may allow studies of cell transitions and migration behavior mimicking matrix rearrangement processes frequently observed during development, cancer, fibrosis and degenerative diseases. Additionally, a recent study using cylindrical wires observed high curvatures can also influence cell detachments at the front edge of epithelial monolayers [54]. We believe this platform can be potentially extended to fibers and non-planar surfaces to test the dynamic of cell detachments under irregular surfaces by combining the precise control of laser photo-activation.

In summary, this novel approach allowed by using a photo-activatable cell adhesive ligand, reveals a fiber-dependent single cell migration of endothelial monolayers. Extension of this experimental approach to study cell migration under dynamic ECM conditions by *in situ* adjustment of the geometry of the migration lines is possible. Our strategy allows advanced studies of cell-ECM relationship and will allow unraveling the role of spatial confinement and ECM morphology in keeping distinct tissue arrangements *in vivo*, and how their disarrangement cause pathological disorders that result in uncontrolled cell growth and dispersion.

4. Materials and methods

4.1. Surface preparation

Cyclo[RGD(DMNPB)fK] was synthesized as reported [35,52]. N-hydroxysuccinimide (NHS) functionalized NEXTERION® Slide H (Schott) was used to immobilize the cyclo[RGD(DMNPB)fK]. Slides were equilibrated in phosphate buffer and incubated with a solution mix of bovine serum albumin (BSA) and cyclo[RGD(DMNPB)fK] (100:1 weight%) in PBS for 1 h in the dark. The substrate was divided into several wells for the experiments by placing a silicone gasket on the top (SI1a).

4.2. Cell culture

Human umbilical vascular endothelial cells (HUVEC) were grown in M199 basal medium supplemented with L-glutamine (2 mM), penicillin (1000 U/mL), streptomycin (100 mg/L), ECGS supplement, sodium heparin (1 mM) and 20% fetal calf serum (FCS) [48]. HUVEC were used between passages 2 to 6. For cell experiments, cells were harvested using 0.25% trypsin and 1 mM EDTA in Hanks buffer.

4.3. Generation of patterned cell monolayers

Patterned cell monolayer was generated as previously described [42]. The cyclo[RGD(DMNPB)fK]-modified substrates were irradiated with a Xe-lamp coupled to a Polychrome V monochromator (360 nm, 0.6 mW/cm^2; TILL Photonics, Gräfelfing, Germany) for 4 min. A quartz glass slide containing a chrome micropatterned mask (width 600 μm, spacing 400 μm) was placed on the substrates during exposure in order to generate a surface pattern of cyclo [RGD(DMNPB)fK] and cyclo[RGDfK] microareas (SI1b). After that, substrates were rinsed with Milli-Q water and dry with N_2 stream.

4.4. Generation of migration lanes from the cell monolayer

Different line widths were irradiated using a custom-built setup which allows adjustable scanning speed and light intensity at the microscope stage [1]. Line width of the scanned line was controlled by using photo-activatable biotin [44] modified substrates as previously described [6]. The exposed biotin substrates were incubated for 30 min in Cy5-labeled strepavidin (eBioscience) (10 μM) in PBS, followed by extensive washing. Surface patterns were then imaged by confocal microscopy (Leica TCS SP5) and analyzed. Integrity of tracks was indirectly observed by using caged biotin that photolyses under similar conditions that our caged RGD [44]. Line width and ligand density were compared (SI1d) after increasing number of laser scans ($\lambda = 405$ nm, energy $= 0.06$ mJ/μm^2). Homogeneous tracks reach full irradiation above 4 scans with an energy dosage of 0.32 mJ/μm^2. Under this condition, focal adhesions (FAs) were found only on the adhesive line (Fig. SI1e), indicating that the presence of active adhesive ligand and the edge of the tracks are well defined.

After calibration (see results 1), patterned cell monolayers were placed on the microscope stage in an incubation chamber (ibidi Heating system) and lines of 3, 5, 10, 15 μm widths were irradiated perpendicularly starting from the edges of the strips using an energy dosage of 0.32 mJ/μm^2. For culture monitoring, phase contrast images were taken every minute.

4.5. Cell transfection and staining

A vinculin-GFP plasmid was used to image vinculin-containing FAs in live cells [5]. Cells were electroporated with a Lonza transfection kit. At the end of the experiment, cells were fixed in 4% paraformaldehyde in PBS for 5 min. The nuclei were stained with 1 mg/mL DAPI (Sigma–Aldrich) and the actin cytoskeleton was visualized with phalloidin-TRITC (Sigma–Aldrich). The samples were analyzed using confocal (Leica TCS SP5) or epifluorescence (Leica AF7000 widefield with BL-X) microscopy.

4.6. Image analysis, cell tracking and nuclear and body dimensions

Time lapse images were stacked and cells were manually tracking by using FIJI software [43]. Velocity and instantaneous speed was calculated from the average displacement *of* the cell geometric center at every 5 min during a time lapse of at least 6 h. Also, nuclear short and long axes, body dimensions and general image analysis was carried out using FIJI.

4.7. Statistics

Statistics analyses were conducted using OriginPro 9. Kruskal–Wallis test was performed for non-parametric analyses. For multiple comparisons between control and all other samples Dwass-Steel-Critchlow-Fligner post hoc contrast was used. In case of parametric test, one-factor ANOVA and Dunnett's post hoc test was used with 95% of confidence. A statistic box was used to represent the data (at least 6 cells) showing the percentile (25/75) values.

Acknowledgments

The authors thank Dr. Sandra Ritz (Max-Planck Institut für Polymerforschung, Mainz) for help with cell cultures and transfection experiments, Dr. Ronald Unger (RepairLab, University Medical Center Mainz) for providing HUVECs, and Prof. Denis Wirtz (Johns Hopkins University) for helpful discussions. This work was funded by the Materials World Network (DFG AOBJ 569628, NSF DMR-0909002) and the Deutsche Forschungsgemeinschaft (DFG CA 880/4-1). MJS and AdC thank CONICET (D.N° 2332, 2013–2014) and DFG (CA880/4-1) for travelling funding grant. NC thanks the International Max-Planck Research School for funding her research stay.

Appendix A. Supplementary data

Supplementary data related to this article can be found at http://dx.doi.org/10.1016/j.biomaterials.2015.12.001.

References

[1] M. Alvarez, J.M. Alonso, O. Filevich, M. Bhagawati, R. Etchenique, J. Piehler, A. del Campo, Modulating surface density of proteins via caged surfaces and controlled light exposure, Langmuir 27 (2011) 2789–2795.
[2] E.M. Balzer, Z. Tong, C.D. Paul, W.C. Hung, K.M. Stroka, A.E. Boggs, S.S. Martin, K. Konstantopoulos, Physical confinement alters tumor cell adhesion and migration phenotypes, FASEB J. 26 (2012) 4045–4056.
[3] S.S. Chang, W.H. Guo, Y. Kim, Y.L. Wang, Guidance of cell migration by substrate dimension, Biophys. J. 104 (2013) 313–321.
[4] G. Charras, E. Sahai, Physical influences of the extracellular environment on cell migration, Nat. Rev. Mol. Cell Biol. 15 (2014) 813–824.
[5] S.R. Coyer, A. Singh, D.W. Dumbauld, D.A. Calderwood, S.W. Craig, E. Delamarche, A.J. Garcia, Nanopatterning reveals an ECM area threshold for focal adhesion assembly and force transmission that is regulated by integrin activation and cytoskeleton tension, J. Cell Sci. 125 (2012) 5110–5123.
[6] A. del Campo, D. Boos, H.W. Spiess, U. Jonas, Surface modification with orthogonal photosensitive silanes for sequential chemical lithography and site-selective particle deposition, Angew. Chem. Int. Ed. 44 (2005) 4707–4712.
[7] A.D. Doyle, M.L. Kutys, M.A. Conti, K. Matsumoto, R.S. Adelstein, K.M. Yamada, Micro-environmental control of cell migration–myosin IIA is required for efficient migration in fibrillar environments through control of cell adhesion dynamics, J. Cell Sci. 125 (2012) 2244–2256.
[8] A.D. Doyle, R.J. Petrie, M.L. Kutys, K.M. Yamada, Dimensions in cell migration, Curr. Opin. Cell Biol. 25 (2013) 642–649.
[9] A.D. Doyle, F.W. Wang, K. Matsumoto, K.M. Yamada, One-dimensional topography underlies three-dimensional fibrillar cell migration, J. Cell Biol. 184 (2009) 481–490.
[10] E. Fong, S. Tzlil, D.A. Tirrell, Boundary crossing in epithelial wound healing, Proc. Natl. Acad. Sci. U. S. A. 107 (2010) 19302–19307.
[11] P. Friedl, E. Sahai, S. Weiss, K.M. Yamada, New dimensions in cell migration, Nat. Rev. Mol. Cell Biol. 13 (2012) 743–747.
[12] P. Friedl, K. Wolf, Proteolytic and non-proteolytic migration of tumour cells and leucocytes, in: Biochem Soc Symp, 2003, pp. 277–285.
[13] P. Friedl, K. Wolf, Tumour-cell invasion and migration: diversity and escape mechanisms, Nat. Rev. Cancer 3 (2003) 362–374.
[14] P. Friedl, K. Wolf, Plasticity of cell migration: a multiscale tuning model, J. Cell Biol. 188 (2010) 11–19.
[15] P. Friedl, K. Wolf, J. Lammerding, Nuclear mechanics during cell migration, Curr. Opin. Cell Biol. 23 (2011) 55–64.
[16] P. Friedl, K.S. Zanker, E.B. Brocker, Cell migration strategies in 3-D extracellular matrix: differences in morphology, cell matrix interactions, and integrin function, Microsc. Res. Tech. 43 (1998) 369–378.
[17] H. Gerhardt, VEGF and endothelial guidance in angiogenic sprouting, Organogenesis 4 (2008) 241–246.
[18] S. Giampieri, C. Manning, S. Hooper, L. Jones, C.S. Hill, E. Sahai, Localized and reversible TGFbeta signalling switches breast cancer cells from cohesive to single cell motility, Nat. Cell Biol. 11 (2009) 1287–1296.
[19] T. Harada, J. Swift, J. Irianto, J.W. Shin, K.R. Spinler, A. Athirasala, R. Diegmiller, P.C. Dingal, I.L. Ivanovska, D.E. Discher, Nuclear lamin stiffness is a barrier to 3D migration, but softness can limit survival, J. Cell Biol. 204 (2014) 669–682.
[20] B.D. Harms, G.M. Bassi, A.R. Horwitz, D.A. Lauffenburger, Directional persistence of EGF-induced cell migration is associated with stabilization of lamellipodial protrusions, Biophys. J. 88 (2005) 1479–1488.

[21] B. Huang, M. Lu, M.K. Jolly, I. Tsarfaty, J. Onuchic, E. Ben-Jacob, The three-way switch operation of Rac1/RhoA GTPase-based circuit controlling amoeboid-hybrid-mesenchymal transition, Sci. Rep. 4 (2014) 6449.
[22] W.C. Hung, S.H. Chen, C.D. Paul, K.M. Stroka, Y.C. Lo, J.T. Yang, K. Konstantopoulos, Distinct signaling mechanisms regulate migration in unconfined versus confined spaces, J. Cell Biol. 202 (2013) 807–824.
[23] S.B. Khatau, C.M. Hale, P.J. Stewart-Hutchinson, M.S. Patel, C.L. Stewart, P.C. Searson, D. Hodzic, D. Wirtz, A perinuclear actin cap regulates nuclear shape, Proc. Natl. Acad. Sci. U. S. A. 106 (2009) 19017–19022.
[24] D.H. Kim, S. Cho, D. Wirtz, Tight coupling between nucleus and cell migration through the perinuclear actin cap, J. Cell Sci. 127 (2014) 2528–2541.
[25] K. Konstantopoulos, P.H. Wu, D. Wirtz, Dimensional control of cancer cell migration, Biophys. J. 104 (2013) 279–280.
[26] M. Krause, A. Gautreau, Steering cell migration: lamellipodium dynamics and the regulation of directional persistence, Nat. Rev. Mol. Cell Biol. 15 (2014) 577–590.
[27] K.R. Levental, H. Yu, L. Kass, J.N. Lakins, M. Egeblad, J.T. Erler, S.F. Fong, K. Csiszar, A. Giaccia, W. Weninger, M. Yamauchi, D.L. Gasser, V.M. Weaver, Matrix crosslinking forces tumor progression by enhancing integrin signaling, Cell 139 (2009) 891–906.
[28] Y.J. Liu, M. Le Berre, F. Lautenschlaeger, P. Maiuri, A. Callan-Jones, M. Heuze, T. Takaki, R. Voituriez, M. Piel, Confinement and low adhesion induce fast amoeboid migration of slow mesenchymal cells, Cell 160 (2015) 659–672.
[29] P. Lu, K. Takai, V.M. Weaver, Z. Werb, Extracellular matrix degradation and remodeling in development and disease, Cold Spring Harb. Perspect. Biol. 3 (2011).
[30] P. Lu, V.M. Weaver, Z. Werb, The extracellular matrix: a dynamic niche in cancer progression, J. Cell Biol. 196 (2012) 395–406.
[31] L. Maddaluno, N. Rudini, R. Cuttano, L. Bravi, C. Giampietro, M. Corada, L. Ferrarini, F. Orsenigo, E. Papa, G. Boulday, E. Tournier-Lasserve, F. Chapon, C. Richichi, S.F. Retta, M.G. Lampugnani, E. Dejana, EndMT contributes to the onset and progression of cerebral cavernous malformations, Nature 498 (2013) 492–496.
[32] P. Maiuri, E. Terriac, P. Paul-Gilloteaux, T. Vignaud, K. McNally, J. Onuffer, K. Thorn, P.A. Nguyen, N. Georgoulia, D. Soong, A. Jayo, N. Beil, J. Beneke, J.C. Lim, C.P. Sim, Y.S. Chu, W.C.R. participants, A. Jimenez-Dalmaroni, J.F. Joanny, J.P. Thiery, H. Erfle, M. Parsons, T.J. Mitchison, W.A. Lim, A.M. Lennon-Dumenil, M. Piel, M. Thery, The first World Cell Race, Curr. Biol. 22 (2012) R673–R675.
[33] B. Palmgren, Y. Jiao, E. Novozhilova, S.I. Stupp, P. Olivius, Survival, migration and differentiation of mouse tau-GFP embryonic stem cells transplanted into the rat auditory nerve, Exp. Neurol. 235 (2012) 599–609.
[34] K. Pankova, D. Rosel, M. Novotny, J. Brabek, The molecular mechanisms of transition between mesenchymal and amoeboid invasiveness in tumor cells, Cell Mol. Life Sci. 67 (2010) 63–71.
[35] S. Petersen, J.M. Alonso, A. Specht, P. Duodu, M. Goeldner, A. del Campo, Phototriggering of cell adhesion by caged cyclic RGD peptides, Angew. Chem. Int. Ed. 47 (2008) 3192–3195.
[36] R.J. Petrie, A.D. Doyle, K.M. Yamada, Random versus directionally persistent cell migration, Nat. Rev. Mol. Cell Biol. 10 (2009) 538–549.
[37] P.P. Provenzano, K.W. Eliceiri, J.M. Campbell, D.R. Inman, J.G. White, P.J. Keely, Collagen reorganization at the tumor-stromal interface facilitates local invasion, BMC Med. 4 (2006) 38.
[38] S. Raghavan, R.A. Desai, Y. Kwon, M. Mrksich, C.S. Chen, Micropatterned dynamically adhesive substrates for cell migration, Langmuir 26 (2010) 17733–17738.
[39] B. Ranchoux, F. Antigny, C. Rucker-Martin, A. Hautefort, C. Pechoux, H.J. Bogaard, P. Dorfmuller, S. Remy, F. Lecerf, S. Plante, S. Chat, E. Fadel, A. Houssaini, I. Anegon, S. Adnot, G. Simonneau, M. Humbert, S. Cohen-Kaminsky, F. Perros, Endothelial-to-mesenchymal transition in pulmonary hypertension, Circulation 131 (2015) 1006–1018.
[40] K.M. Riching, B.L. Cox, M.R. Salick, C. Pehlke, A.S. Riching, S.M. Ponik, B.R. Bass, W.C. Crone, Y. Jiang, A.M. Weaver, K.W. Eliceiri, P.J. Keely, 3D collagen alignment limits protrusions to enhance breast cancer cell persistence, Biophys. J. 107 (2014) 2546–2558.
[41] P. Roca-Cusachs, J. Alcaraz, R. Sunyer, J. Samitier, R. Farre, D. Navajas, Micropatterning of single endothelial cell shape reveals a tight coupling between nuclear volume in G1 and proliferation, Biophys. J. 94 (2008) 4984–4995.
[42] M.J. Salierno, A.J. Garcia, A. del Campo, Photo-activatable surfaces for cell migration assays, Adv. Funct. Mater. 23 (2013) 5974–5980.
[43] J. Schindelin, I. Arganda-Carreras, E. Frise, V. Kaynig, M. Longair, T. Pietzsch, S. Preibisch, C. Rueden, S. Saalfeld, B. Schmid, J.Y. Tinevez, D.J. White, V. Hartenstein, K. Eliceiri, P. Tomancak, A. Cardona, Fiji: an open-source platform for biological-image analysis, Nat. Methods 9 (2012) 676–682.
[44] S. Sundberg, R. Barrett, C. Holmes, Spatially-addressable immobilization of macromolecules on solid substrates, FASEB J. 6 (1992). A171–A171.
[45] C.H. Thomas, J.H. Collier, C.S. Sfeir, K.E. Healy, Engineering gene expression and protein synthesis by modulation of nuclear shape, Proc. Natl. Acad. Sci. U. S. A. 99 (2002) 1972–1977.
[46] S. Tojkander, G. Gateva, P. Lappalainen, Actin stress fibers–assembly, dynamics and biological roles, J. Cell Sci. 125 (2012) 1855–1864.
[47] V.M. Tysseling, V. Sahni, E.T. Pashuck, D. Birch, A. Hebert, C. Czeisler, S.I. Stupp, J.A. Kessler, Self-assembling peptide amphiphile promotes plasticity of serotonergic fibers following spinal cord injury, J. Neurosci. Res. 88 (2010) 3161–3170.
[48] R.E. Unger, V. Krump-Konvalinkova, K. Peters, C.J. Kirkpatrick, In vitro expression of the endothelial phenotype: comparative study of primary isolated cells and cell lines, including the novel cell line HPMEC-ST1.6R, Microvasc. Res. 64 (2002) 384–397.
[49] S.R. Vedula, H. Hirata, M.H. Nai, A. Brugues, Y. Toyama, X. Trepat, C.T. Lim, B. Ladoux, Epithelial bridges maintain tissue integrity during collective cell migration, Nat. Mater 13 (2014) 87–96.
[50] S.R. Vedula, M.C. Leong, T.L. Lai, P. Hersen, A.J. Kabla, C.T. Lim, B. Ladoux, Emerging modes of collective cell migration induced by geometrical constraints, Proc. Natl. Acad. Sci. U. S. A. 109 (2012) 12974–12979.
[51] M. Versaevel, T. Grevesse, S. Gabriele, Spatial coordination between cell and nuclear shape within micropatterned endothelial cells, Nat. Commun. 3 (2012) 671.
[52] M. Wirkner, S. Weis, V. San Miguel, M. Alvarez, R.A. Gropeanu, M. Salierno, A. Sartoris, R.E. Unger, C.J. Kirkpatrick, A. del Campo, Photoactivatable caged cyclic RGD peptide for triggering integrin binding and cell adhesion to surfaces, Chembiochem 12 (2011) 2623–2629.
[53] K. Wolf, M. Te Lindert, M. Krause, S. Alexander, J. Te Riet, A.L. Willis, R.M. Hoffman, C.G. Figdor, S.J. Weiss, P. Friedl, Physical limits of cell migration: control by ECM space and nuclear deformation and tuning by proteolysis and traction force, J. Cell Biol. 201 (2013) 1069–1084.
[54] H.G. Yevick, G. Duclos, I. Bonnet, P. Silberzan, Architecture and migration of an epithelium on a cylindrical wire, Proc. Natl. Acad. Sci. U. S. A. 112 (2015) 5944–5949.
[55] E.M. Zeisberg, S. Potenta, L. Xie, M. Zeisberg, R. Kalluri, Discovery of endothelial to mesenchymal transition as a source for carcinoma-associated fibroblasts, Cancer Res. 67 (2007) 10123–10128.
[56] A. Zemel, F. Rehfeldt, A.E. Brown, D.E. Discher, S.A. Safran, Cell shape, spreading symmetry and the polarization of stress-fibers in cells, J. Phys. Condens Matter 22 (2010) 194110.
[57] X. Zhou, R.G. Rowe, N. Hiraoka, J.P. George, D. Wirtz, D.F. Mosher, I. Virtanen, M.A. Chernousov, S.J. Weiss, Fibronectin fibrillogenesis regulates three-dimensional neovessel formation, Genes Dev. 22 (2008) 1231–1243.